Optical sensor array of metal-organic-framework-based inverse opal films for the detection and identification of various alcohols

Kuo Zhan [a,b], Peng Qin [a], Yunzhe Jiang [a], Yunlin Chen [b], Lars Heinke [a,*]

[a] Karlsruhe Institute of Technology (KIT), Institute of Functional Interfaces (IFG), Hermann-von-Helmholtz-Platz 1, Eggenstein-Leopoldshafen 76344, Germany
[b] Beijing Jiaotong University (BJTU), School of Physical Science and Engineering, Beijing 100044, China

ARTICLE INFO

Keywords:
Optical sensor array
Inverse opal structures
Surface-mounted metal-organic frameworks
Vapor detection

ABSTRACT

Reliable and inexpensive sensors for the detection and discrimination of various volatile organic compounds like different alcohols are required for many applications, for example to proof the alcohol quality and for avoiding methanol poising. Here, we develop a sensor array of films made of different types of surface-mounted metal-organic frameworks (SURMOFs) with a periodic three-dimensional structure of mesoscopic voids, referred to as inverse opal structure. The wavelength shift (or alternatively, the intensity change) of the photonic reflectance peak caused by the analyte vapor adsorption in the SURMOF was used as signal. The sensor array is applied for the detection of various pure low-carbon alcohols, which are methanol, ethanol, 1-propanol, and 1-butanol. The sensor array shows a low limit of detection (LOD) in the range of 10–60 ppm and is able to reliably discriminate the alcohols from each other. Furthermore, the sensor array is able to precisely discriminate their pure vapors and binary mixtures with methanol. We foresee such sensor array with SURMOF-based inverse opal films offer a great potential for the precise and cost-efficient detection of various analytes.

1. Introduction

Methanol poisoning can cause severe health problems such as blindness, permanent neurologic dysfunction, and even death [1,2]. For example, more than 5000 methanol poisonings were reported in Iran, Turkey, and India in 2019 [3–5]. Toxic alcohol poisoning can be associated with a significant degree of morbidity and mortality if not promptly recognized and treated after the accidental and non-accidental exposures [6]. Toxic components, including methanol, propanol, isopropyl alcohol and butanol [7,8], can be widely found in homemade alcoholic beverages. Therefore, it is crucial to detect the concentration and identify the types of alcohol vapors safely and precisely. This needs to be realized by cost-efficient, reliable, and available sensors. So far, only limited research in this field has been reported.

Metal-organic frameworks (MOFs) are a class of nanoporous crystalline hybrid materials, which possess numerous distinct features, including high porosity, high specific surface area and diversified structures [9,10]. Based on the versatile host-guest interaction and the large surface area, MOF films have been used in various sensor applications [11–16]. MOF thin films can also be made in a layer-by-layer fashion, resulting in surface-mounted metal-organic frameworks (SURMOFs) [17,18]. To date, SURMOF films have been used in single optical sensor such as one-dimensional photonic crystals (Braggs stacks) sensors [19,20] and Fabry-Perot cavity sensors [21]. Sensor arrays based on SURMOFs of different structures in combination with a gravimetric quartz crystal microbalance have been used to detect and identify various volatile compounds [22–24].

An opal structure is a periodic three-dimensional mesoscopic alignment of materials with different dielectric constants, like a regular closed-packed assembly of identical spheres [25,26]. An inverse opal structure is a regular three-dimensional mesoscopic structure of voids, i.e. it is inverse to the opal structure [27,28]. The characteristic dimensions of an opal or inverse opal structure are in the order of visible light. Light is diffracted by such an opal structure and the optical properties are very sensitive to the change in its refractive index (RI), see supporting information (SI) [29,30]. Since the RI can be altered by the uptake of guest molecules, the incorporation of porous materials, like SURMOFs, into such a photonic material will provide a general signal transduction scheme for the development of optical sensors. This results in portable, label-free, room temperature vapor/gas sensors. (Label-free refers to sensors without colorimetric labels, such as functionalized nanoparticles with strong, specific adsorption sites, where the sensor

* Corresponding author.
E-mail address: Lars.Heinke@KIT.edu (L. Heinke).

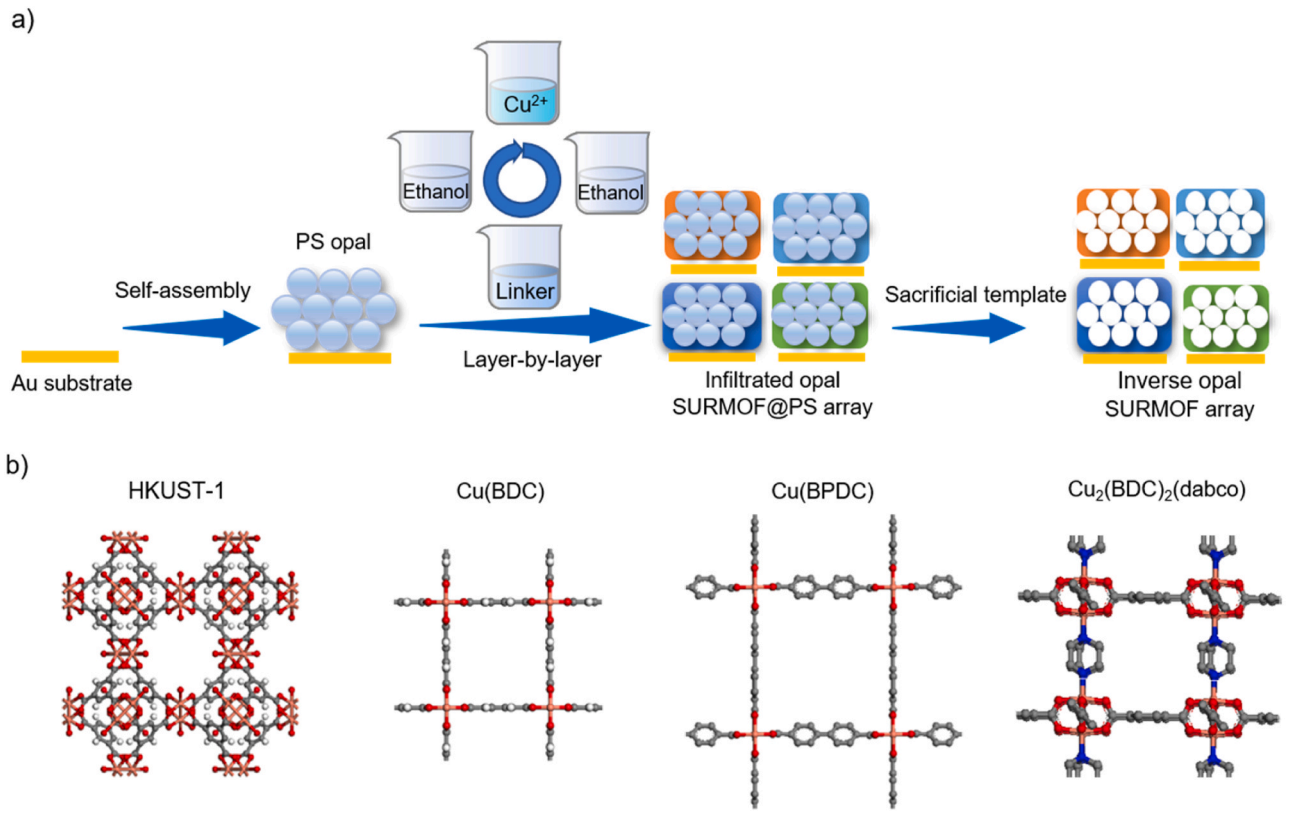

Fig. 1. : a) The synthesis of the SURMOF-based-inverse-opal film array. **b)** Sketches of the SURMOFs structures: HKUST-1, Cu(BDC) SURMOF-2, Cu(BPDC) SURMOF-2 and $Cu_2(BDC)_2(dabco)$, left to right, see labels.

response is typically not reversible.) For example, a single inverse-opal-film made of MOFs like HKUST-1 has been used for the detection of different organic vapors [31]. ZIF-8 has also been applied in a inverse-opal film for the sensing of linear alcohols homologs analytes [28]. A MOF-based inverse-opal sensor array, able to detect and discriminate various analytes and mixtures, has not yet been presented.

Herein, we present the first optical sensor array of SURMOF-based inverse opal films. The array is composed of four sensors made of different SURMOF films with structures of type HKUST-1 [31], Cu(BDC) [32], Cu(BPDC) [32] and $Cu_2(BDC)_2(dabco)$ [33]. The MOF structures were chosen because of their high porosity and good stability [31]. The pore size of the MOF films is in between 0.6 nm and 1.5 nm [31–34]. Moreover, the synthesis procedures for preparing thin homogenous films of these MOFs with a low defect density in a layer-by-layer fashion at mild conditions are known [35–37]. The inverse opal structure films are made by employing polystyrene spheres (PS) as opal templates for the SURMOFs growth. To fabricate the SURMOF-inverse-opal-structure films, the PS films are employed as sacrificial opal template for the SURMOF growth. Subsequently, the PS spheres were dissolved to form the inverse opal MOF structure. The characteristic dimensions of the periodic opal or inverse opal structure are in the order of the wavelength of visible light, causing photonic properties of the film. These photonic properties are highly sensitive to changes of the refractive index (RI) of the film (see SI), which is affected by the uptake of guest molecules in the MOF pores. Thus, the exposures and uptake of analyte molecules affects the photonic properties of the MOF film with the inverse opal structure. These changes of the photonic properties (i.e. the shift of the wavelength and of the intensity of the photonic reflectance peaks) are used as sensor signals. Taking advantage of the photonic properties of the inverse opal films and the sensitivity to the changes of the refractive index, the SURMOF-inverse-opal-array is used as sensor system for the detection and discrimination of volatile molecules. Here, we explore the sensor response to alcoholic analytes, which are methanol (MeOH), ethanol (EtOH), 1-propanol (PrOH), and 1-butanol (BuOH) in their pure form as well as of their binary mixtures with MeOH. The sensor array data are analyzed by applying established machine learning algorithms like k-Nearest Neighbor (k-NN) [38,39], Support Vector Method (SVM) [20] and Artificial Neural Network (ANN) [40]. As result, the sensor array is able to identify all alcohol analytes and their binary mixtures with very high accuracy. The sensors also show a very low limit of detection in the range of 10–60 ppm.

2. Synthesis

The synthesis of the SURMOF-based-inverse-opal film sensor array is outlined in Fig. 1. First, COOH-terminated polystyrene nanospheres (PS) with a diameter of 350 nm were dispersed in deionized water and deposited on Au-coated silicon wafer substrates to form an opal structure film (PS opal film) using an evaporation-induced self-assembly approach, see ref. [41]. Second, the SURMOFs were grown on the PS-opal film in a stepwise layer-by-layer fashion. This was performed by alternatively exposing the PS-opal film to the metal node and linker solutions via a dipping-robot method [35] to construct the SURMOF@PS-infiltrated-opal films. For synthesizing the different SURMOF structures, different components were used. While all used SURMOFs are based on copper-dimer-nodes (the metal node solution was 0.2 mM ethanolic copper acetate solution), ethanolic linker solutions were trimesic acid (BTC, 0.1 mM) for HKUST-1, terephthalic acid (BDC, 0.1 mM) for Cu(BDC), biphenyl dicarboxylic acid (BPDC, 0.1 mM) for Cu(BPDC) and mixed terephthalic acid and 1,4-diazabicyclo[2.2.2]octane (BDC and dabco, each 0.1 mM) for $Cu_2(BDC)_2(dabco)$. Finally, the SURMOF-based-inverse-opal films were obtained after removing the PS spheres in a tetrahydrofuran solution. More details are given in the Supporting Information (SI).

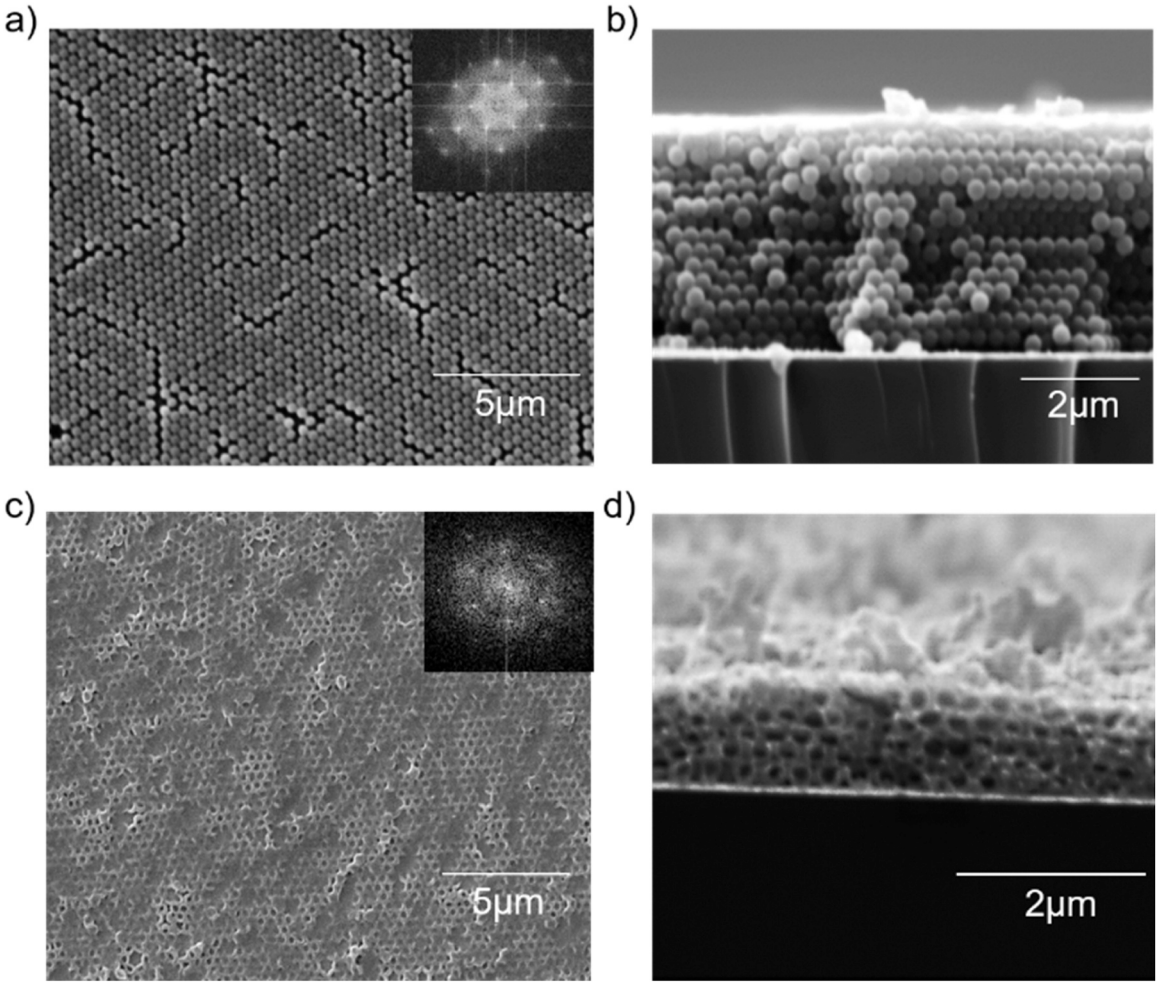

Fig. 2. : The SEM images of the PS-opal template film (**a** and **b**) and of the HKUST-1-inverse-opal film (**c** and **d**). The top view (**a** and **c**) and the cross section (**b** and **d**) of the broken samples are shown. The insets in **a**) and **c**) show the Fourier transformations of the images.

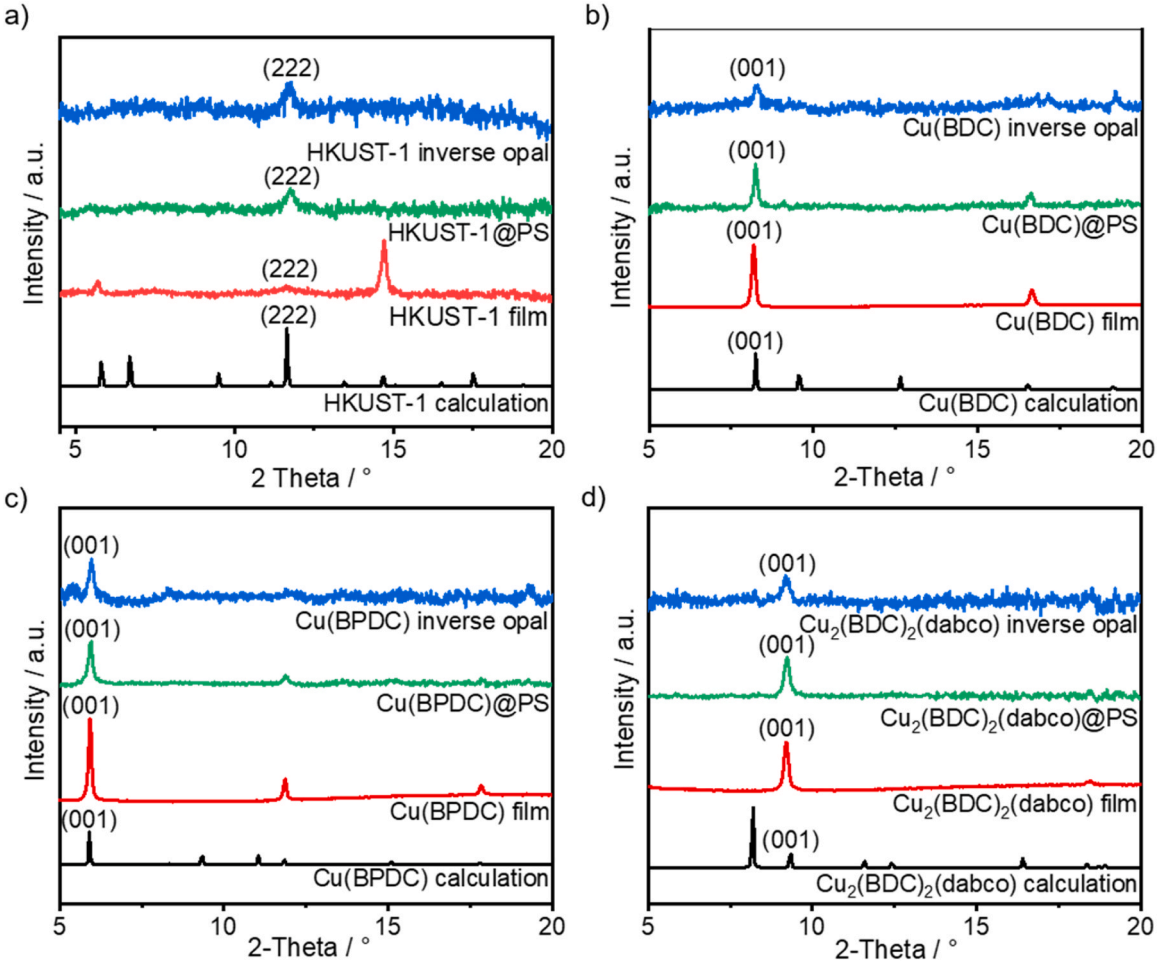

Fig. 3. : X-ray diffractograms of the SURMOF-inverse-opal films, SURMOF-infiltrated-opal films, pure SURMOF films and compared with the calculated structures for **a)** HKUST-1, **b)** Cu(BDC) SURMOF-2, **c)** Cu(BPDC) SURMOF-2 and **d)** $Cu_2(BDC)_2(dabco)$. The diffraction peaks observed for the SURMOF-inverse-opal films are labelled.

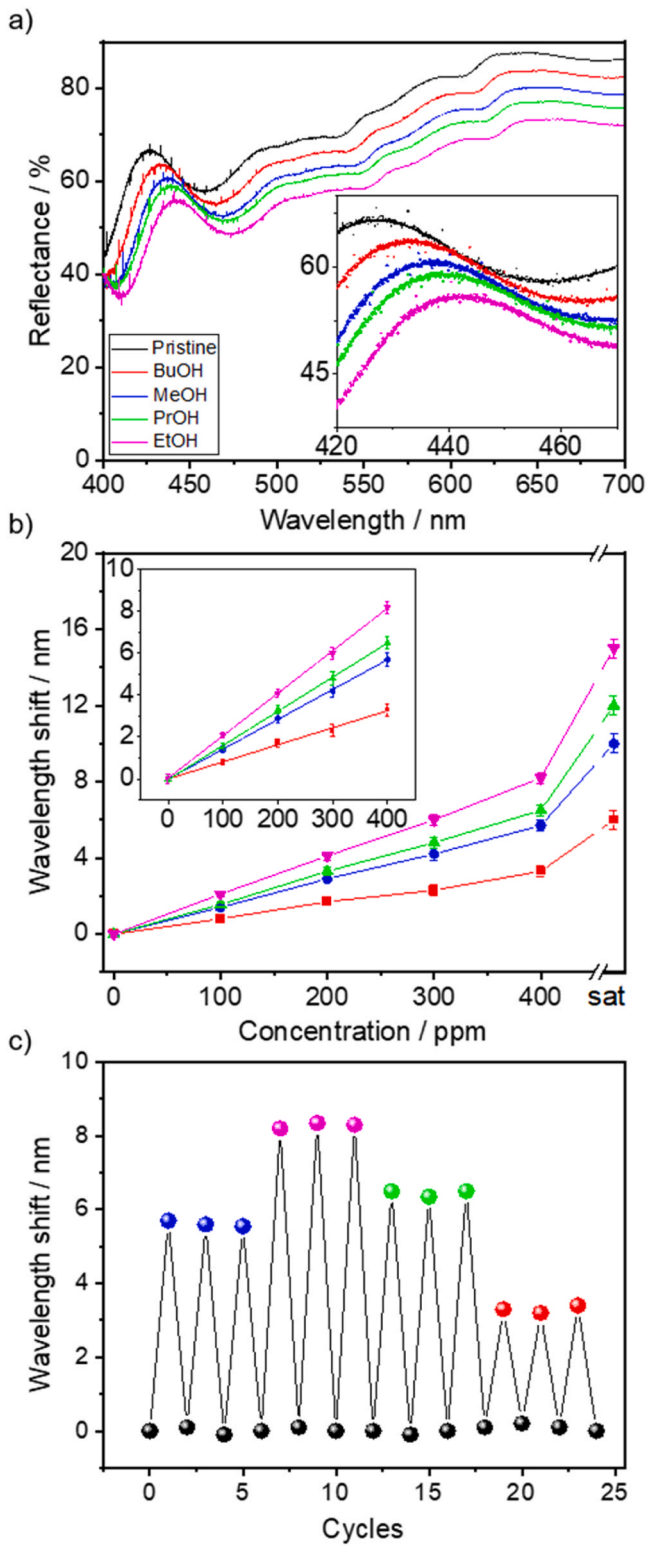

Fig. 4. a) The reflectance spectra of the HKUST-1-inverse-opal film in an atmosphere of saturated alcohol vapors, see labels. **b)** The wavelength shift of the reflectance peak of the HKUST-1-inverse-opal film (at ~427.6 nm) *versus* concentration. The inset shows the reflectance wavelength shift with the linear fits, where the slopes represent the wavelength sensitivity. The same color code as in panel a) is used. **c)** The repeatability test of the HKUST-1-inverse-opal film for the exposure to 400 ppm of different alcohols, see labels in a).

3. Characterization

The PS-opal template film is imaged by scanning electron microscopy (SEM) in Fig. 2a and b. The PS film has a face-centered-cubic (FCC) structure and a (111) crystalline orientation perpendicular to the substrate surface. The Fourier transformation of the SEM image (inset in Fig. 2a) also verifies the regular structure.

The SEM images of the HKUST-1-inverse-opal structure (where the sacrificial PS template was removed) are shown in Fig. 2c and d. The voids in the inverse-opal-structure have approximately the same diameter as the PS-spheres of the template (d=350 nm). This indicates the successful replication of the template structure. SEM images of the HKUST-1@PS-infiltrated-opal film (before removing PS) and other SURMOF-inverse-opal-films are displayed in Fig. S3.

The crystalline structures of the SURMOFs in the inverse-opal-films are explored by X-ray diffraction (XRD) analysis, Fig. 3. The XRD data show that the SURMOF films in the inverse-opal-structure (as well as in the infiltrated-opal structure, i.e. before removing the PS) are crystalline and the films have the targeted structures as shown in Fig. 1b.

The infrared reflection absorption spectra (IRRAS) of the PS opal film, the pure SURMOF films, the SURMOF-infiltrated-opal films and the SURMOF-inverse-opal-films are shown in Fig. S2. The part of the spectra in the range of 3200–2800 cm^{-1} represents the region of the C-H stretching vibrations in PS. The peaks at 3082, 3060, 3062, 2923, and 2848 cm^{-1} correspond to the aromatic C-H stretching vibrations and the asymmetric and symmetric stretching vibrations of methylene groups -CH_2- [42,43]. Most important, the absence of these bands in the inverse-opal-samples indicate the PS removal, while the SURMOF vibration bands are still present in the inverse-opal samples.

4. Sensor properties

The photonic properties of the inverse-opal can be described by the Bragg equation, see SI [27,28]. The main reflectance wavelength and reflectance intensities are sensitive to the changes in lattice parameters and the average refractive index (RI). Upon exposure to the vapors of the analytes, the analyte molecules diffuse into the MOF material. The analyte uptake increases the RI of the SURMOF-inverse-opal film, shifting the reflectance to larger wavenumbers.

First, the sensing performance was tested for the pure alcohol analytes. The reflectance spectra of the HKUST-1-inverse-opal film, either empty (pristine) or exposed to the saturated vapors of four different alcohols, are shown in Fig. 4a. (The vapor pressures of the analytes are given in Table 1.) The wavelengths of the reflectance peaks of the empty (pristine) sensors are ~428 nm for HKUST-1, ~422 nm for $Cu_2(BDC)_2(dabco)$, ~436 nm for Cu(BDC)-SURMOF-2 and ~438 nm for Cu(BPDC)-SURMOF-2. The wavelength shifts (as well as the intensity changes) of these peaks are used as sensor signals.

The reflectance wavelength shift and reflectance intensity changes in the sensor are caused by the analyte adsorption in the SURMOF-inverse-opal films. Three major factors govern the size of the sensor response: the RIs of the analytes (1.328 of MeOH < 1.361 of EtOH < 1.384 of PrOH < 1.399 of BuOH) [44,45], the molecular size (MeOH < EtOH < PrOH < BuOH) and the polarity (MeOH > EtOH > PrOH > BuOH). The wavelength shift of the photonic reflectance peak of the HKUST-1-inverse-opal film *versus* analyte concentration are shown in Fig. 4b. The sensitivities, determined from the slopes, are given in Table 1. The calculated LODs are in between 10 and 60 ppm. Moreover, its excellent repeatability caused by the reversible uptake and release is demonstrated in Fig. 4c. The data for the SURMOF-inverse-opal-film sensors based on Cu(BDC) SURMOF-2, Cu(BPDC) SURMOF-2, $Cu_2(BDC)_2(dabco)$ are shown in Fig. S3~S9, the parameters are also shown in Table 1. Noteworthy, each sensor shows a different sensitivity for the same analyte vapor, and different analytes exhibit different sensitivities in the same sensor.

Table 1
Sensor parameters: wavelength and intensity sensitivity and LOD of the SURMOF-inverse-opal films for the pure alcohols. The LODs are calculated by $3\sigma/s$, where σ is the standard deviation of the baseline (i.e. from 3 blank measurements, which is determined to be ~0.1 nm for the wavelength-analysis and ~0.01 % for the intensity-analysis) and s is the respective sensitivity). The saturated vapor pressures of the analytes are also shown.

	SURMOF	Wavelength-sensitivity in 10^{-2} nm / ppm	Wavelength-LOD in ppm	Intensity-sensitivity in 10^{-4} / ppm	Intensity-LOD in ppm
Methanol (MeOH)	HKUST-1	1.4	21.4	–0.7	42.9
p_{sat} = 16.7 kPa	Cu(BDC)	1.5	20	–1.2	25
	Cu(BPDC)	1.8	16.7	–1.0	30
	$Cu_2(BDC)_2(dabco)$	1.8	16.7	–0.6	50
Ethanol (EtOH)	HKUST-1	2.0	15	–0.9	33.3
p_{sat} = 7.96 kPa	Cu(BDC)	1.2	25	–1.0	30
	Cu(BPDC)	1.6	18.75	–0.8	37.5
	$Cu_2(BDC)_2(dabco)$	2.8	10.7	–1.2	25
1-Propanol (PrOH)	HKUST-1	1.6	18.75	–0.8	37.5
p_{sat} = 2.78 kPa	Cu(BDC)	1.0	30	–0.8	37.5
	Cu(BPDC)	1.2	25	–0.7	42.9
	$Cu_2(BDC)_2(dabco)$	2.0	15	–0.8	37.5
1-Butanol (BuOH)	HKUST-1	0.8	37.5	–0.5	60
p_{sat} = 0.73 kPa	Cu(BDC)	0.7	42.9	–0.6	50
	Cu(BPDC)	1.0	30	–0.5	60
	$Cu_2(BDC)_2(dabco)$	1.2	25	–0.4	75

In addition to using the wavelength shift (with the determined wavelength-sensitivity and wavelength-LOD), the intensity of the reflectance peak was used as sensor response. There the determined parameters are referred to as intensity-sensitivity and intensity-LOD, see Table 1. Noteworthy, the data show that the method based on the wavelength results in somewhat higher sensitivities and lower LODs.

The radar plot of the wavelength shifts of the SURMOF-inverse-opal-sensors in different alcohol vapors at 100 ppm is shown in Fig. 5a. In the radar plot, each analyte has a different shape, presenting its characteristic pattern or fingerprint. Therefore, their identification is principally possible.

Further radar plots for the wavelength shifts at different concentrations are shown in Fig. S10. The radar plot of the wavelength-sensitivity of the SURMOF-inverse-opal-sensor-array in the different alcohol vapors is shown in Fig. 5b. Noteworthy, since the wavelength-shift is essentially proportional to the analyte concentration (as expected for small concentrations, i.e. in the Henry region), the shape of the radar plots of the same analyte at different concentrations are identical (only the scale of the radar plots are different). Due to the linear change of the wavelength (or reflectance intensity, see e.g. Fig. 4b or S9c), once the type of alcohol is determined (e.g. from the characteristic shape in the radar plot), its concentration can be determined.

For a detailed quantification of the sensing data and for a performance investigation, the data were analyzed by simple machine learning algorithms. Here, we used k-NN, SVM and ANN and we used the data from the intensity change of the reflectance peak. The confusion matrices, summarizing the performance of the classification algorithm for the test data, are shown in Fig. 5b and Fig. S11–S13. Fig. 5b shows the quantitative classifications of the pure alcohols vapors at a concentration of 100 ppm by k-NN. The average classification accuracy is 95.4 %, indicating a high discrimination accuracy for the pure alcohol vapors. Different machine learning algorithms, i.e. SVM and ANN, result in similar results, Figs. S14 and S15.

The sensing performance of the SURMOF-inverse-opal-sensor-array toward mixtures of alcohol vapors was also investigated. To this end, the sensor response to binary alcohol mixtures of MeOH and either EtOH, PrOH or BuOH, each with a concentration of 200 ppm, compared to pure alcohols of 400 ppm was explored, Fig. S16. The Radar plot of the wavelength shifts and the classification confusion matrix of the sensor data are shown in Fig. 6. The average classification accuracy is 96.1 %, indicating a high classification accuracy for the identification of these pure and binary mixture vapors.

In comparison to existing optical alcohol sensors in the literature, the SURMOF-inverse-opal-sensor-array exhibits a great sensing performance, in particular with respect to the sensitivity, detection limits and discrimination capabilities among different types of alcohols. Details are show in table S2. The anti-interference ability and repeatability of the sensors are given in table S1.

5. Conclusion

A sensor array based on films with inverse-opal-structures made of different nanoporous MOFs has been presented. The MOF structures were prepared in a layer-by-layer fashion. Here, the sensor is composed of 4 different SURMOF structures, all based on copper-dimers connected by different short linker molecules. The photonic properties are responsive to the analyte uptake by the SURMOFs, thus, the change of the wavelength as well as the change of the intensity of the reflectance peak can be used as optical sensor signal. The sensor array was applied for the detection and discrimination of four volatile alcohols. The sensor array shows very high sensitivities and very low limits of detection in the range of 10–60 ppm. Moreover, the different pure alcohols can be distinguished by their unique pattern in the radar plots. Machine learning algorithms show that the alcohols can be classified with very high accuracies of more than 90 %. Moreover, binary 1:1 alcohol mixtures were also identified from pure vapors and from each other with high classification accuracies.

This study shows that simple and inexpensive optical sensors based on SURMOF-inverse-opal-films provide a sufficient sensitivity and repeatability for detecting different alcohols and their mixtures. While we focused here on various alcohols, we believe the present study is the ideal starting point for exploring also the response to many different analytes, like esters, acetone, ether and water and many more, either in their pure form or as mixtures. We foresee that increasing the number of sensors and using specialized SURMOFs with more specific host-guest interaction towards the targeted molecules will provide a new approach toward the application of MOF-based optical sensors to detect and identify various targeted molecules at room temperature.

CRediT authorship contribution statement

KZ performed the experiments and analyzed the data with the support of PQ and YC. KZ prepared the SURMOF-inverse-opal films. YJ

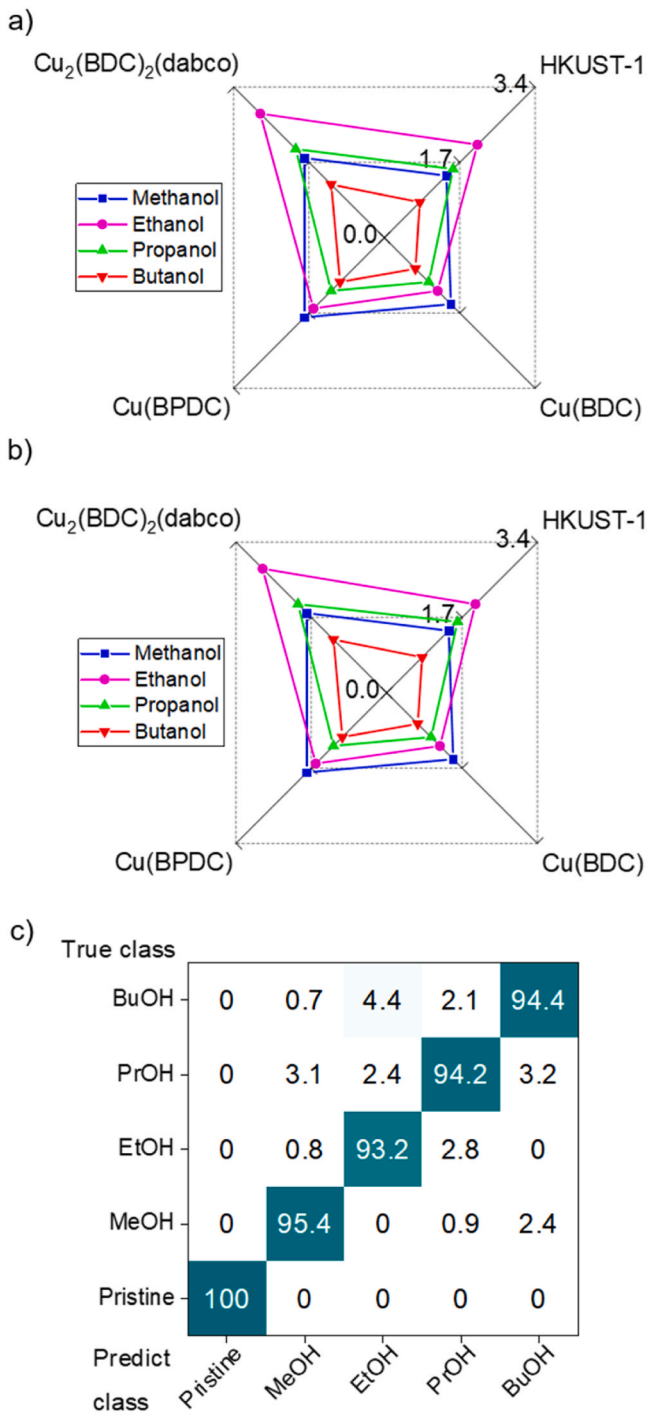

Fig. 5. a) Radar plot of the wavelength shift of the SURMOF-inverse-opal-sensor-array in the analyte vapors with a concentration of 100 ppm. The units of the axes are nm. **b)** Radar plot of the wavelength sensitivity of the SURMOF-inverse-opal-sensor-array. The units of the axes are 10^{-2} nm / ppm. **c)** The classification confusion matrix for the pure alcohol vapors at a concentration of 100 ppm and the pristine sample. The pristine sample (with empty pores) is obtained upon desorbing the analytes in a flow of pure nitrogen at room temperature for at least 2 h. The matrix is determined by k-NN. The true classes are the rows and the predicted classes are the columns. The accuracies of the classification of the data are shown in the matrix. The numbers are in percent. Correct classifications are on the matrix's main diagonal; misclassifications are the other values.

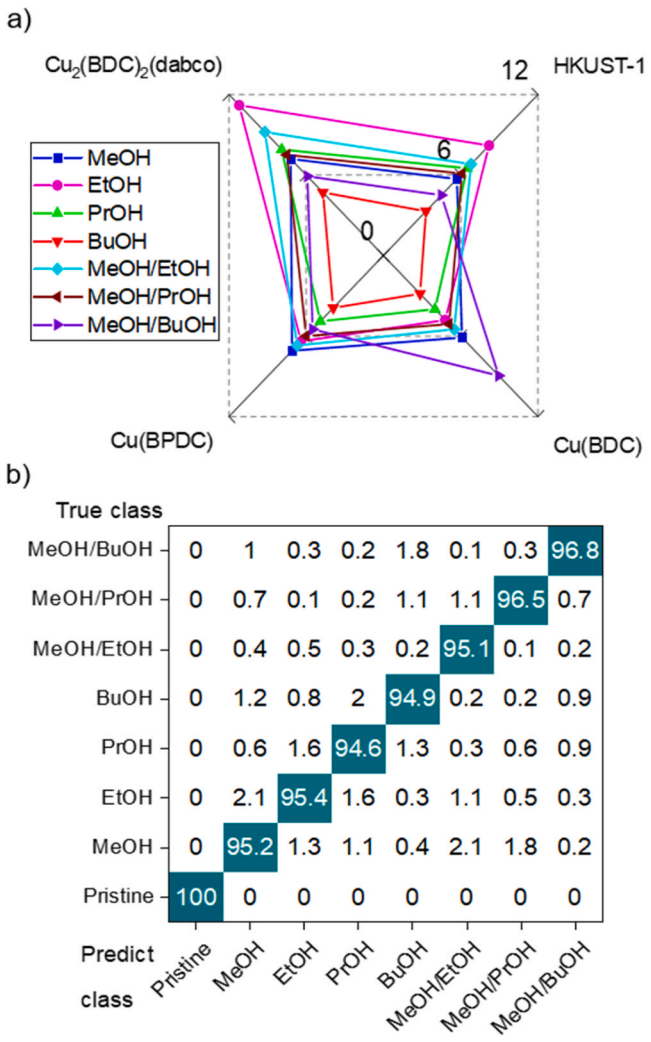

Fig. 6. a) Radar plot of the reflectance intensity changes of the SURMOFs inverse opal film sensor array for binary mixture vapors (200 ppm + 200 ppm) and pure vapors (400 ppm). **b)** The classification confusion matrix. The data were calculated by k-NN. The numbers are in percent.

measured the SEM images. KZ and LH planned the project and experiments. KZ and LH wrote the manuscript. All authors supported and approved the manuscript.

Declaration of Competing Interest

The authors report no declarations of interest.

Data Availability

Data will be made available on request.

Acknowledgments

The authors acknowledge financial support from the Deutsche Forschungsgemeinschaft (DFG, via SPP 1928 COORNETs and via HE 7036/5), the Fundamental Research Funds for the Central Universities 20211YJS175, the China Scholarship Council (CSC).

References

[1] J. Kruse, Methanol poisoning, Intensive Care Med. 18 (1992) 391–397.
[2] P.D. Bryson, Comprehensive Reviews in Toxicology: For Emergency Clinicians, CRC press,, 1996.
[3] P. Pressman, R. Clemens, S. Sahu, A.W. Hayes, A review of methanol poisoning: a crisis beyond ocular toxicology, Cutan. Ocul. Toxicol. 39 (3) (2020) 173–179.
[4] M. Shokoohi, N. Nasiri, H. Sharifi, S. Baral, S. Stranges, A syndemic of COVID-19 and methanol poisoning in Iran: Time for Iran to consider alcohol use as a public health challenge? Alcohol 87 (2020) 25–27.
[5] M. Gulen, S. Satar, A. Avci, S. Acehan, U. Orhan, H. Nazik, Methanol poisoning in Turkey: two outbreaks, a single center experience, Alcohol 88 (2020) 83–90.
[6] C. Wang, D. Samaha, S. Hiremath, L. Sikora, M.M. Sood, S. Kanji, E.G. Clark, Outcomes after toxic alcohol poisoning: a systematic review protocol, Syst. Rev. 7 (1) (2018) 1–7.
[7] P.C.Y. Ng, W.T. Davis, D.J. Sessions, A. Koyfman, Toxic alcohol diagnosis and management: an emergency medicine review, Intern. Emerg. Med. 13 (2018) 375–383.
[8] N. Gallagher, F.J. Edwards, The diagnosis and management of toxic alcohol poisoning in the emergency department: a review article, Adv. J. Emerg. Med. 3 (3) (2019).
[9] H. Furukawa, K.E. Cordova, M. O'Keeffe, O.M. Yaghi, The chemistry and applications of metal-organic frameworks, Science 341 (6149) (2013), 1230444.
[10] S. Kaskel, The Chemistry of Metal-Organic Frameworks, 2vol Set: Synthesis, Characterization, and Applications, Vol. 1, John Wiley & Sons,, 2016.
[11] I. Stassen, N.C. Burtch, A.A. Talin, P. Falcaro, M.D. Allendorf, R. Ameloot, An updated roadmap for the integration of metal-organic frameworks with electronic devices and chemical sensors, Chem. Soc. Rev. 46 (12) (2017), 3853-3853.
[12] I. Strauss, A. Mundstock, M. Treger, K. Lange, S. Hwang, C. Chmelik, P. Rusch, N. C. Bigall, T. Pichler, H. Shiozawa, J. Caro, Metal-organic framework Co-MOF-74-based host-guest composites for resistive gas sensing, ACS Appl. Mater. Int. 11 (15) (2019) 14175–14181.
[13] A. Chidambaram, K.C. Stylianou, Electronic metal-organic framework sensors, Inorg. Chem. Front. 5 (5) (2018) 979–998.
[14] V. Pentyala, P. Davydovskaya, M. Ade, R. Pohle, G. Urban, Metal-organic frameworks for alcohol gas sensor, Sens. Actuators B-Chem. 222 (2016) 904–909.
[15] A.L. Robinson, V.L. Stavila, T.R. Zeitler, M.I. White, S.M. Thornberg, J. A. Greathouse, M.D. Allendorf, Ultrasensitive humidity detection using metal-organic framework-coated microsensors, Anal. Chem. 84 (16) (2012) 7043–7051.
[16] F.M. Hinterholzinger, A. Ranft, J.M. Feckl, B. Ruhle, T. Bein, B.V. Lotsch, One-dimensional metal-organic framework photonic crystals used as platforms for vapor sorption, J. Mater. Chem. 22 (20) (2012) 10356–10362.
[17] O. Shekhah, H. Wang, S. Kowarik, F. Schreiber, M. Paulus, M. Tolan, C. Sternemann, F. Evers, D. Zacher, R.A. Fischer, Step-by-step route for the synthesis of metal organic frameworks, J. Am. Chem. Soc. 129 (49) (2007) 15118–15119.
[18] L. Heinke, C. Wöll, Surface-mounted metal–organic frameworks: crystalline and porous molecular assemblies for fundamental insights and advanced applications, Adv. Mater. 31 (26) (2019), 1806324.
[19] Z. Zhang, K. Müller, S. Heidrich, M. Koenig, T. Hashem, T. Schlöder, D. Bleger, W. Wenzel, L. Heinke, Light-switchable one-dimensional photonic crystals based on MOFs with photomodulatable refractive index, J. Phys. Chem. Lett. 10 (21) (2019) 6626–6633.
[20] J. Liu, E. Redel, S. Walheim, Z. Wang, V. Oberst, J. Liu, S. Heissler, A. Welle, M. Moosmann, T. Scherer, Monolithic high performance surface anchored metal organic framework Bragg reflector for optical sensing, Chem. Mater. 27 (6) (2015) 1991–1996.
[21] Z. Li, J. Liu, X. Yi, W. Wu, F. Li, Z. Zhu, H. Li, J. Shi, Y. Xu, F. Zhou, Metal–organic frameworks-based Fabry Pérot cavity encapsulated TiO2 nanoparticles for selective chemical sensing, Adv. Funct. Mater. 32 (9) (2022), 2109541.
[22] S. Okur, P. Qin, A. Chandresh, C. Li, Z. Zhang, U. Lemmer, L. Heinke, An enantioselective e-nose: an array of nanoporous homochiral MOF films for stereospecific sensing of chiral odors, Angew. Chem. Int. Ed. 60 (7) (2021) 3566–3571.
[23] P. Qin, S. Okur, C. Li, A. Chandresh, D. Mutruc, S. Hecht, L. Heinke, A photoprogrammable electronic nose with switchable selectivity for VOCs using MOF films, Chem. Sci. 12 (47) (2021) 15700–15709.
[24] P. Qin, B.A. Day, S. Okur, C. Li, A. Chandresh, C.E. Wilmer, L. Heinke, VOC mixture sensing with a MOF film sensor array: detection and discrimination of xylene Isomers and their ternary blends, ACS Sens. 7 (6) (2022) 1666–1675.
[25] J.H. Moon, S. Yang, Chemical aspects of three-dimensional photonic crystals, Chem. Rev. 110 (1) (2010) 547–574.
[26] R.K. Cersonsky, J. Antonaglia, B.D. Dice, S.C. Glotzer, The diversity of three-dimensional photonic crystals, Nat. Commun. 12 (1) (2021) 2543.
[27] Y.-n Wu, F. Li, Y. Xu, W. Zhu, C.-a Tao, J. Cui, G. Li, Facile fabrication of photonic MOF films through stepwise deposition on a colloid crystal substrate, Chem. Commun. 47 (36) (2011) 10094–10096.
[28] Y. n Wu, F. Li, W. Zhu, J. Cui, C. a Tao, C. Lin, P.M. Hannam, G. Li, Metal–organic frameworks with a three-dimensional ordered macroporous structure: dynamic photonic materials, Angew. Chem. 123 (52) (2011) 12726–12730.
[29] M. Nankali, Z. Einalou, M. Asadnia, A. Razmjou, High-sensitivity 3D ZIF-8/PDA photonic crystal-based biosensor for blood component recognition, ACS Appl. Bio Mater. 4 (2) (2021) 1958–1968.
[30] S. Qin, S. Zhang, M. Chen, L. Wu, Electrochemical fabrication of long-range ordered macro-microporous metal–organic framework films, J. Mater. Chem. A 10 (17) (2022) 9497–9505.
[31] S.S.-Y. Chui, S.M.-F. Lo, J.P. Charmant, A.G. Orpen, I.D. Williams, A chemically functionalizable nanoporous material [Cu3 (TMA) 2 (H2O) 3] n, Science 283 (5405) (1999) 1148–1150.
[32] J. Liu, B. Lukose, O. Shekhah, H.K. Arslan, P. Weidler, H. Gliemann, S. Bräse, S. Grosjean, A. Godt, X. Feng, A novel series of isoreticular metal organic frameworks: realizing metastable structures by liquid phase epitaxy, Sci. Rep. 2 (1) (2012) 921.
[33] O. Shekhah, Layer-by-layer method for the synthesis and growth of surface mounted metal-organic frameworks (SURMOFs), Materials 3 (2) (2010) 1302–1315.
[34] M. Cakici, Z.-G. Gu, M. Nieger, J. Bürck, L. Heinke, S. Bräse, Planar-chiral building blocks for metal–organic frameworks, Chem. Commun. 51 (23) (2015) 4796–4798.
[35] Z.-G. Gu, A. Pfriem, S. Hamsch, H. Breitwieser, J. Wohlgemuth, L. Heinke, H. Gliemann, C. Wöll, Transparent films of metal-organic frameworks for optical applications, Microporous Mesoporous Mater. 211 (2015) 82–87.
[36] Z. Wang, K. Müller, M. Valášek, S. Grosjean, S. Bräse, C. Wöll, M. Mayor, L. Heinke, Series of photoswitchable azobenzene-containing metal–organic frameworks with variable adsorption switching effect, J. Phys. Chem. C. 122 (33) (2018) 19044–19050.
[37] L. Heinke, C. Wöll, Surface-mounted metal–organic frameworks: crystalline and porous molecular assemblies for fundamental insights and advanced applications, Adv. Mater. 31 (26) (2019), 1806324.
[38] S. Okur, Z. Zhang, M. Sarheed, P. Nick, U. Lemmer, L. Heinke, Towards a MOF e-nose: a SURMOF sensor array for detection and discrimination of plant oil scents and their mixtures, Sens. Actuators B: Chem. 306 (2020), 127502.
[39] V. Schroeder, E.D. Evans, Y.-C.M. Wu, C.-C.A. Voll, B.R. McDonald, S. Savagatrup, T.M. Swager, Chemiresistive sensor array and machine learning classification of food, ACS Sens. 4 (8) (2019) 2101–2108.
[40] M.G. Xibilia, M. Latino, Z. Marinković, A. Atanasković, N. Donato, Soft sensors based on deep neural networks for applications in security and safety, IEEE Trans. Instrum. Meas. 69 (10) (2020) 7869–7876.
[41] A.S. Dimitrov, K. Nagayama, Continuous convective assembling of fine particles into two-dimensional arrays on solid surfaces, Langmuir 12 (5) (1996) 1303–1311.
[42] B. Hanulikova, T. Capkova, J. Antos, M. Urbanek, P. Urbanek, J. Sevcik, I. Kuritka, Temperature dependence of vibrational motions of thin polystyrene films by infrared reflection-absorption spectroscopy: a single measurement tool for monitoring of glass transition and temperature history, Polym. Test. 101 (2021), 107305.
[43] D. Olmos, E. Martín, J. González-Benito, New molecular-scale information on polystyrene dynamics in PS and PS–BaTiO 3 composites from FTIR spectroscopy, Phys. Chem. Chem. Phys. 16 (44) (2014) 24339–24349.
[44] J. Ortega, Densities and refractive indices of pure alcohols as a function of temperature, J. Chem. Eng. Data 27 (3) (1982) 312–317.
[45] D. Weimer, L. Lindemuth, W. Groves, Refractive index of alcohol nonionics, J. Am. Oil Chemists' Soc. 44 (3) (1967) 171–174.